Structure and magnetic properties of Fe/V (110) superlattices

P. Isberg
Department of Physics, Uppsala University, S-751 21 Uppsala, Sweden

P. Granberg
Department of Materials Science, Uppsala University, S-751 21 Uppsala, Sweden

E. B. Svedberg
Department of Physics, Linköping University, S-581 83 Linköping, Sweden

B. Hjörvarsson and R. Wäppling
Department of Physics, Uppsala University, S-751 21 Uppsala, Sweden

P. Nordblad
Department of Materials Science, Uppsala University, S-751 21 Uppsala, Sweden
(Received 3 March 1997; revised manuscript received 22 October 1997)

Structural, magnetic, and magnetotransport properties of Fe/V (110) superlattices have been investigated. Using Al_2O_3 (1120) substrates and Mo or Mo_xV_{1-x} alloy seed layers, the superlattices could be grown with a large in- and out-of-plane crystal coherence. Due to large strains, magnetoelastic effects give rise to a uniaxial in-plane magnetocrystalline anisotropy with the [001] direction as the easy axis. The anisotropy energy of the strained Fe layers was found to be of similar magnitude as the one of bulk Co. The magnetotransport properties were investigated on a series of superlattice films with the nominal structure Al_2O_3/Mo (100 Å)/[Fe (23 Å)/V $(4-23$ Å$)]_{20}$. For V thicknesses below 15 Å, only anisotropic magnetoresistance effects are present. For larger thicknesses giant magnetoresistance effects are also present, indicating antiferromagnetic coupling across the V interlayers. The interplay between the magnetic anisotropy, hysteresis effects, and the antiferromagnetic coupling is discussed. [S0163-1829(98)06506-0]

INTRODUCTION

The magnetic properties of magnetic multilayers have been the subject of numerous studies in recent years. Magnetic phenomena such as oscillating exchange coupling,[1] giant magnetoresistance (GMR),[2] and surface anisotropy[3] have been extensively investigated. A close relationship between the structure and the magnetic properties has been demonstrated, one example being the influence of the interface roughness on the GMR.[4] Furthermore, theoretical and experimental studies have shown that both the magnetic exchange coupling across the interlayer and the magnetic interface anisotropy are dependent on the crystal orientation.[5,6] The heteroepitaxial growth of superlattices with different crystallographic orientations inevitably leads to lattice strain which may vary substantially between the different growth directions.[6] Therefore, the observed orientation dependence of the magnetic properties could in many cases arise from a strain induced magnetic anisotropy. To distinguish between a magnetoelastic effect and an intrinsic orientation dependent magnetic property, further investigations of the relations between the structural and the magnetic properties are required.

Magnetic properties of textured Fe/V multilayers have been investigated previously, but no orientation dependence of the intrinsic magnetic properties has been reported. In a recent paper on single crystal bct Fe/V (001) superlattices,[7] a ferromagnetic behavior for vanadium thicknesses in the range 1–14 monolayers was reported. The in-plane magnetic anisotropy showed a clear dependence on the V thickness, arising from magnetoelastic effects associated with different lattice strains. Later it was shown that Fe/V (001) superlattices exhibits antiferromagnetic coupling for structures with thin Fe (3 ML) and V thicknesses in the range of 12–14 ML.[8] Previous investigations have shown that Fe/V (110) superlattices can be grown on single-crystal MgO (111) wafers at 200 °C with a large out-of-plane crystal coherence (~400 Å) (Ref. 9) but no reports regarding magnetic properties on Fe/V (110) superlattices have been published. However, results obtained on polycrystalline samples with {110} texture, indicate a weak oscillatory antiferromagnetic coupling[10] and a small GMR arising from hysteresis effects.[11]

This paper reports on the structure and magnetic properties of Fe/V (110) superlattices. It was found that the system can be grown with a large in-plane and out-of-plane crystal coherence. Magnetization measurements, using superconducting quantum interference device (SQUID) magnetometry, show that the Fe layers exhibit an uniaxial magnetic anisotropy. We will argue that these effects arise from misfit induced strain of the constituents. Magnetoresistance measurements also show that the system exhibits GMR for V layer thicknesses around 20 Å, indicating antiferromagnetic (AF) coupling between successive Fe layers at those thicknesses.

EXPERIMENT

The Fe/V multilayers were fabricated in a three source ultrahigh vacuum (UHV) based sputtering system[12] with base pressure below 1×10^{-9} Torr (1.33×10^{-7} Pa). The substrates, single-crystal Al_2O_3 (1120) wafers, were ultrasonically precleaned in isopropanol and ethanol, loaded into the deposition system and thereafter annealed at 700 °C for 20 min. High purity Ar (99.9999%) gas with a partial pressure of 5.0×10^{-3} Torr was used in the sputtering process yielding typical deposition rates of 0.5 and 0.7 Å/s for V and Fe, respectively, monitored by quartz crystal microbalances. The samples were rotated (50–100 rpm) during deposition to prevent thickness gradients.

Some of the Fe/V multilayers were grown directly on the substrate and others on seed layers of different thicknesses and compositions. All seed layers were deposited at 700 °C. A number of samples with the same nominal structure, Al_2O_3(1120)/Mo 200 Å/$Mo_{1-x}V_x$ alloy 200 Å/[Fe 30 Å/V 20 Å]$_{20}$, were prepared at different temperatures (20–330 °C) in order to find the optimum growth temperature. During the growth of the $Mo_{1-x}V_x$ alloy seed layer x was continuously increased from 0 to 1. The purpose of using an alloy seed layer was to gradually decrease the in-plane lattice parameter in order to improve the epitaxial growth of the Fe/V multilayers.

Two samples with the nominal structures, Al_2O_3 (1120)/Mo 200 Å/[Fe 31 Å/V 17 Å]$_{60}$ and Al_2O_3 (1120)/Mo 200 Å/$Mo_{1-x}V_x$ alloy 200 Å/[Fe 23 Å/V 16 Å]$_{40}$, grown at 180 °C, were used for an extensive investigation of the structural and magnetic properties. To investigate the magnetotransport properties of Fe/V (110), a series of samples with the following sequence, Al_2O_3 (1120)/Mo 100 Å/[Fe 23 Å/V d Å]$_{40}$ where $4<d<23$ Å was prepared. All samples were covered with a 100 Å thick cap layer of V to protect the multilayer structure from oxidation upon exposure to air.

The structural quality of the samples was investigated by *in situ* reflective high energy electron diffraction (RHEED) and by conventional $\theta-2\theta$ x-ray diffraction (XRD) (Cu$K\alpha$ radiation) using a powder diffractometer with a resolution of 0.005° in 2θ. The XRD measurements were carried out in a low-angle region (1°–12° in 2θ) as well as in a high-angle region (30°–55° in 2θ) around the Fe/V (110) Bragg peak. Scans to search for additional Bragg peaks were also performed in a larger region (10°–120° in 2θ). Reciprocal space mapping (RSM) was performed, using a Philips MRD system, around the Fe/V (110), (222), and (310) Bragg peaks, to determine the in- and out-of-plane lattice parameter. Corrections for miscut and diffractometer offsets were determined from the (1120) reflection of the Al_2O_3 substrate and the (110) reflection of the Fe/V multilayer. To deduce the epitaxy and to determine the texture of the samples, {222} and {200} pole figures from the film as well as {1126} and {3030} pole figures from the Al_2O_3 substrate were recorded.

The magnetic properties were investigated using a Quantum Design 5.5 T SQUID magnetometer. The samples were cut in rectangular pieces with the edges of the Al_2O_3 substrate parallel to the [001] and [110] in-plane directions of the Fe/V film. All measurements were performed with the magnetic field applied in the plane of the samples. The magnetoresistive measurements were carried out in a Lake-Shore 7225 series Susceptometer/Magnetometer system. A dc current of 1 mA was applied in the film plane giving a current density of approximately 10^7 A/m^2 and the magnetoresistance was measured with the field directed along the in-plane [001] and [110] directions. To investigate the influence of the anisotropic magnetoresistance on the magnetotransport properties, measurements were performed with the current parallel and perpendicular to the magnetic field.

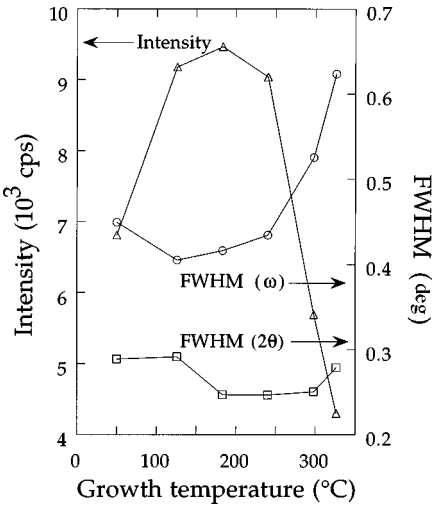

FIG. 1. The intensity and the FWHM in ω (rocking curve) and 2θ of the (110) Bragg peak as a function of the growth temperature of the Fe (30 Å)/V (20 Å) multilayers grown on 200 Å Mo/200 Å Mo_xV_{1-x} seed layer.

RESULT AND DISCUSSION

A. Structural properties

The XRD measurements revealed that the growth of Fe/V ML's directly on the Al_2O_3 (1120) wafers, independent of the growth temperature, resulted in polycrystalline samples with a fairly poor {110} texture. When using seed layers of Mo or Mo/$Mo_{1-x}V_x$, it was found that an improved crystalline quality could be obtained. In Fig. 1 the results from XRD measurements on Fe (30 Å)/V (20 Å) ML's grown at different temperatures on a Mo/$Mo_{1-x}V_x$ seed layer are shown. As can be seen, the intensity of the (110) Bragg peak is strongly dependent on the growth temperature and has a maximum value at 180 °C. At this growth temperature, the full width half maximum (FWHM) of the (110) Bragg peak has a minimum value in 2θ, as well as in ω (rocking curve). The temperature for optimum crystal ordering (180 °C) is also typical for the Fe/V multilayers grown on Mo seed layers. Compared to samples grown on the alloy seed layer the intensity of the (110) Bragg peak in these samples is slightly reduced and a small increase of the FWHM (in ω and 2θ) of the (110) Bragg peak is found. A gradual deterioration of the crystal quality with decreasing thickness of the Mo seed layer was also observed.

The structural quality of one of the samples, the Fe (31 Å)/V (17 Å) multilayer grown on a 200 Å Mo seed layer at 180 °C, was thoroughly investigated using different structural characterization methods. RHEED patterns of the sample surface were measured *in situ* both after deposition of

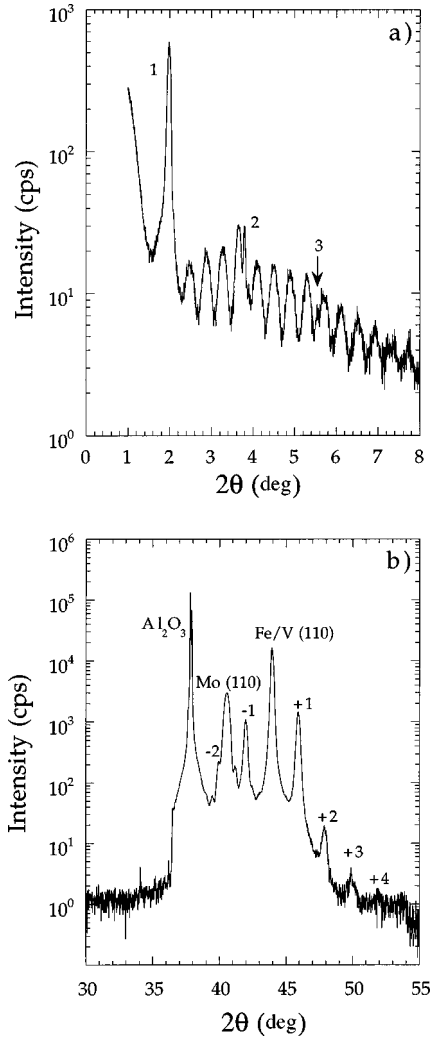

FIG. 2. (a) Low-angle reflectivity curve for Fe (31 Å)/V (17 Å) film grown at 180 °C on 200 Å Mo seed layer. The broader interference peaks arise from the Mo seed layer. Three peaks arising from the chemical modulation are indicated. (b) High-angle x-ray diffraction data. To the left of the Fe/V (110) Bragg peak is the Mo seed layer (110) Bragg peak, with corresponding Laue oscillations. The indices above the curves identify the order of the satellites.

the 200 Å Mo seed layer and after the last deposited Fe layer. The Mo (110) surface showed a high order reconstruction. The (110) surface mesh of Mo was nonuniformly expanded, with the mesh expanded more in the in-plane [001] direction than in the [110] direction. The RHEED patterns of the Fe (110) surface showed a mixture of a 2D streak pattern superimposed on a 3D point pattern which indicates an island growth. Comparison between the lattice distance in the [001] and [110] directions indicated, as in the case of Mo, a slightly larger expansion (compared to Fe bulk values) in the [110] direction. Due to the presence of magnetic fields (from the magnetrons) affecting the electron beam, only comparative measurements of the in-plane lattice parameter were performed.

In Fig. 2, spectra from XRD measurements on the Fe (31 Å)/V (17 Å) sample are plotted in the low-angle region [Fig. 2(a)] and the high-angle region [Fig. 2(b)]. The spectrum obtained from the low-angle XRD investigation displays sharp multilayer peaks with low intensity. From the position of the peaks, the modulation wavelength of the sample was determined to 48.1 Å, which is consistent with the result from the high-angle XRD measurements. Simulation of the reflectivity data, using the program GIXA,[13] gives an average interface roughness of the order of 4 Å, which corresponds approximately to 2 atomic layers. In the high-angle region, a well defined (110) Bragg peak with relatively high intensity and well resolved satellites is found. The FWHM (in 2θ) was determined to 0.145° which gives, using the Scherrer formula,[14] an out-of-plane coherence length of 650 Å corresponding to $\frac{1}{4}$ of the total thickness of the multilayer. No additional Bragg peaks, except for the (220) peak, were found in the region 10°–120° (in 2θ).

Figure 3 shows reciprocal space maps of the (110), (222), and (310) reflections from the Fe (31 Å)/V (17 Å) multilayer. In the subsequent calculation of the lattice parameters, consideration has been given to both miscut of the substrate and misalignment of the sample in the diffractometer. The (110) peak is measured twice, once for each of the optimized asymmetric peaks (222) and (310), without changing the tilt or rotation of the sample. From the RSM maps the atomic plane distances for the multilayer were found to have the following values: $d_{[110]}=2.056\pm0.003$ Å, $d_{[001]}=1.462\pm0.003$ Å, and $d_{[1\bar{1}0]}=2.073\pm0.003$ Å. Note that $d_{[110]}$ represents the average out-of-plane atomic plane distance of Fe and V and since essentially no lattice relaxation of the in-plane parameters (of the multilayer film) was observed, the $d_{[001]}$ and $d_{[1\bar{1}0]}$ value can be considered as representative of the in-plane atomic distances of Fe and V. Thus, the same lattice distortion in the two in-plane crystal directions is found ($d_{[1\bar{1}0]}/d_{[001]}=\sqrt{2}$). This result disagrees with the result from the *in situ* RHEED analysis. Since an *ex situ* XRD experiment reflects the average lattice parameter

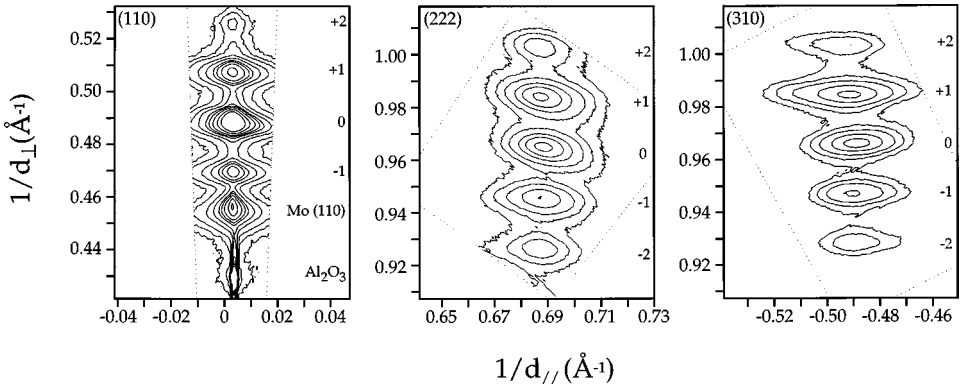

FIG. 3. RSM of the (110), (222), and (310) reflections of the Fe (31 Å)/V (17 Å) film. The numbers indicate the order of the satellites. The isointensity contours are 100, 200, 400, 1000, 2000, 4000, 6000, 10 000, 20 000, and 40 000 counts, respectively.

through the whole multilayer and the RHEED pattern is characteristic only of the surface layer(s), at one particular point during the deposition, such a discrepancy is comprehensible. To fully describe the microstructural changes throughout the thickness of the film, further investigations, using, e.g., transmission electron microscopy, are required.

From the reciprocal space mapping, the in-plane crystal coherence length was determined to 300 Å. Both the in-plane and out-of-plane values (650 Å) of the crystal coherence are considered as lower limits since the instrumental broadening, strain effects, and interfacial roughness all contribute to the line width. The values of the in-plane and out-of-plane crystal coherence are much larger than the modulation period which confirm the superlattice nature of the sample. The {200} pole figure for the Fe/V SL shows two peaks separated by 180° as expected for a (110) oriented bcc single crystal. No additional peaks were found in the region 0°–85° (Ψ) indicating the absence of high-angle grain boundaries. Using additional results from pole figures of the {222} Bragg peaks from Fe/V and the {1126} and {3030} Bragg peaks from the Al_2O_3 substrate the epitaxial relationship between film and substrate could be determined as

$$\mathrm{Fe/V}[110]\|\mathrm{Mo}[110]\|\mathrm{Al_2O_3}[1\bar{1}20],$$

$$\mathrm{Fe/V}[\bar{1}11]\|\mathrm{Mo}[\bar{1}11]\|\mathrm{Al_2O_3}[0001],$$

$$\mathrm{Fe/V}[\bar{1}12]\|\mathrm{Mo}[\bar{1}12]\|\mathrm{Al_2O_3}[\bar{1}100].$$

This epitaxial relationship has also been found when growing, e.g., high quality bcc Nb films onto Al_2O_3 (1120).[15]

In summary, results from the different structural characterization methods show that the superlattices have a good crystal ordering. The optimum crystal quality is obtained by depositing the Fe/V multilayers on a $\mathrm{Mo/Mo}_{1-x}\mathrm{V}_x$ seed layer at a growth temperature of 180 °C. Growing the Fe/V on pure Mo seed layers yields a slightly reduced crystal quality, however, giving an in- and out-of-plane crystal ordering that still by far exceeds the modulation period. The Fe/V (110) superlattice is subject to a nonuniform strain giving a crystal structure that deviates quite significantly from cubic symmetry. In view of the results from other low symmetry magnetic systems,[16] a uniaxial magnetocrystalline anisotropy in the Fe/V (110) superlattice is expected.

B. Magnetic properties

Figure 4 shows magnetization loops measured at 10 K for two Fe/V superlattices grown on different seed layers. The two curves correspond to measurements with the magnetic field applied along the two in-plane [001] and [110] directions. As can be seen, both samples show an in-plane uniaxial magnetocrystalline anisotropy with the [110] direction as the hard direction. For both samples, the magnetization loop in the easy [001] direction is squarelike with a remanent magnetization value corresponding approximately to the saturation magnetization. The only difference between the samples in the easy direction is a small variation in the coercivity. In the hard [110] direction, on the other hand, a significant difference between the samples is seen. For the Fe (31 Å)/V (17 Å) superlattice grown on a 200 Å Mo seed layer [Fig. 4(a)] the magnetization increases linearly with

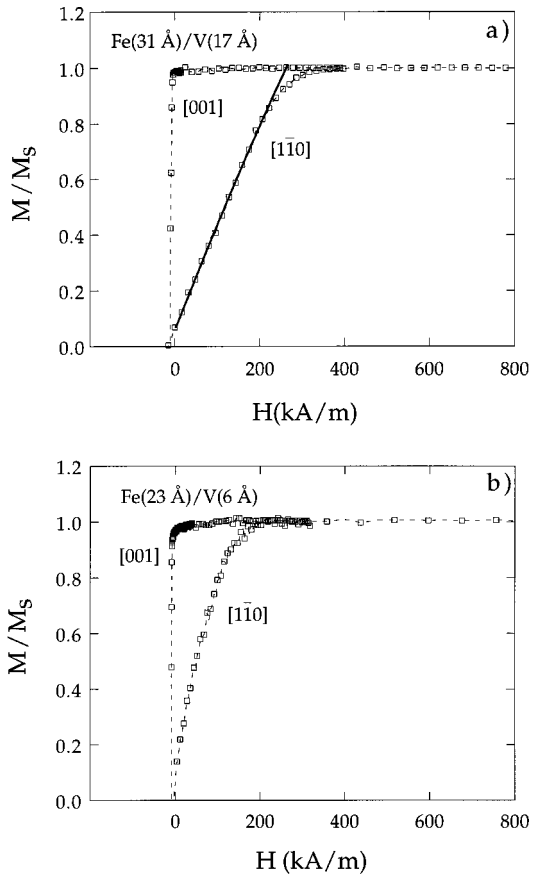

FIG. 4. Reduced magnetization (squares) M/M_s, at $T=10$ K vs applied magnetic field in the in-plane [001] and [110] directions for two Fe/V (110) superlattices. (a) Fe (31 Å)/V (17 Å) grown on Mo (200 Å) and (b) Fe (23 Å)/V (6 Å) grown on Mo (100 Å). Also plotted in (a) is the calculated magnetization curve (solid thick line) in the [110] direction.

applied field and reaches saturation at $H_s \approx 330$ kA/m. The Fe (23 Å)/V (6 Å) superlattice grown on a 100 Å Mo seed layer [Fig. 4(b)] displays a similar uniaxial behavior, but the magnetization shows a curved increase with applied field. Such a nonlinear increase of the magnetization was found for all samples grown on the thin seed layers. No systematic variation of the curvature or of the anisotropy field with the thickness of the V interlayer was found.

The coercivity in the easy ($H_c^{[001]}$) and the hard direction ($H_c^{[1\bar{1}0]}$) as well as the saturation field (H_s) for all samples in the investigation are given in Table I. There is a significant variation of the coercivities and the behavior of the magnetization loops between the different samples. The nonlinear increase of the magnetization can be ascribed mainly to structural defects. The XRD studies have shown that a thin seed layer or a slight variation from the ideal growth condition during the film deposition introduce crystalline defects in the superlattice and results in an increased interface roughness. These defects can introduce strain relaxation in the samples leading to a distribution of anisotropy fields which results in a nonlinear increase of the magnetization with applied magnetic field. Only samples that were grown on a sufficiently thick Mo or $\mathrm{Mo/Mo}_x\mathrm{V}_{1-x}$ seed layer are representative for the highest crystal quality and show a linear increase of the magnetization with applied field. This result

TABLE I. Magnetization data. The following parameters are listed: the thickness of the vanadium spacer (L_v), the coercive field in the easy ($H_c^{[001]}$) and hard ($H_c^{[1\bar{1}0]}$) directions, the saturation field (H_s), and the seed layer in the respective sample.

L_v (Å)	$H_c^{[001]}$ (kA/m)	$H_c^{[1\bar{1}0]}$ (kA/m)	H_s (kA/m)	Seed layer
4.3	8.8			100 Å Mo
6.4	9.2	4.2	200	100 Å Mo
9.6	11.2	14.2	200	100 Å Mo
10.7	13	10.7	160	100 Å Mo
12.8	14.2	10.3	318	100 Å Mo
15	14.9	5	330	100 Å Mo
16	9.2	6.8	330	200 Å Mo/ 200 Å Mo_xV_{1-x}
17	11	16	330	200 Å Mo
17.1	26.3	9	318	100 Å Mo
19.3	31.4	24.7	330	100 Å Mo
20.3	15	14.2	330	100 Å Mo

is consistent with the result from the XRD study which shows that the samples grown on thick Mo or Mo/Mo_xV_{1-x} seed layers give the optimal structural quality.

In order to quantify the anisotropic behavior, we consider a magnetic system with a uniaxial magnetocrystalline anisotropy energy E_a expressed as

$$E_a(\theta)=K_1\sin^2\theta+K_2\sin^4\theta, \tag{1}$$

where K_1 and K_2 are the first and second order uniaxial anisotropy constants and θ is the angle of the magnetization vector with respect to the easy direction of the sample.

The equilibrium condition between the reduced magnetization M/M_s and an external field H applied in the hard [110] direction leads to the following condition:

$$\left(\frac{2K_1}{\mu_0 M_s}\right)\frac{M}{M_s}+\frac{4K_2}{\mu_0 M_s}\left(\frac{M}{M_s}\right)^3=H. \tag{2}$$

The M versus H curve can be fitted using the reduced magnetization in the range $0<M/M_s<1$, $\mu_0 M_s=2.2$ T, and K_1 and K_2 as free parameters. The fitted magnetization curve in the [110] direction is plotted for the Fe (31 Å)/V (17 Å) sample in Fig. 4(a). The best fit to the experimental data gives $K_1=330$ kJ/m^3, $K_2=5$ kJ/m^3. The value of the anisotropy energy is 25 times larger than the low temperature value for bulk iron (13 kJ/m^3) (Ref. 17) and is of the same order of magnitude as the low temperature value of the anisotropy energy for cobalt (700 kJ/m^3).[18]

As was shown in Fig. 4, the Fe/V (110) superlattices possess a large in-plane uniaxial magnetocrystalline anisotropy with the [001] direction as the easy axis. This anisotropy can be ascribed to the reversed magnetostriction produced by the internal strain in the superlattice. Due to the lattice misfit between Fe and V, the Fe layers are subjected to tensile strain both in the [001] and the [110] direction. The XRD investigations have shown that the relative expansion of the Fe layers in the two orientations is approximately the same ($\approx 2\%$) which implies that the ratio between the atomic plane distances in the $[1\bar{1}0]$ and [001] directions equals the equilibrium bulk value $d_{[1\bar{1}0]}/d_{[001]}=\sqrt{2}$.

In a magnetic system that is subject to a resulting stress, σ, an additional term arising from the magnetoelastic energy is added to the total anisotropy energy. In a system with cubic symmetry the total anisotropy energy E_a is given by[19]

$$\begin{aligned}E_a=&K(\alpha_1^2\alpha_2^2+\alpha_2^2\alpha_3^2+\alpha_3^2\alpha_1^2)\\&-\frac{3}{2}\lambda_{100}\sigma(\alpha_1^2\gamma_1^2+\alpha_2^2\gamma_2^2+\alpha_3^2\gamma_3^2)\\&-3\lambda_{111}\sigma(\alpha_1\alpha_2\gamma_1\gamma_2+\alpha_2\alpha_3\gamma_2\gamma_3+\alpha_3\alpha_1\gamma_3\gamma_1),\end{aligned} \tag{3}$$

where K is the first order anisotropy constant for cubic symmetry, λ_{001} and λ_{111} are the magnetoelastic constants in the indicated crystalline directions, and $\{\alpha_i\}$ and $\{\gamma_i\}$ are the direction cosines for the magnetization vector and the stress, respectively. The Fe film is subjected to a tensile stress ($\sigma>0$) both in the [110] direction ($\gamma_1=1\sqrt{2}$, $\gamma_2=-1/\sqrt{2}$, $\gamma_3=0$) and in the [001] direction ($\gamma_1=\gamma_2=0$, $\gamma_3=1$). The following energy terms, therefore, contribute to the magnetoelastic energy:

$$E_{001}=\frac{3}{2}\lambda_{001}\sigma(\sin^2\theta-1)$$

and

$$E_{1\bar{1}0}=-\frac{3}{4}\sigma(\lambda_{001}+\lambda_{111})\sin^2\theta,$$

where θ is the angle in the (110) plane between the magnetization vector and the easy [001] direction. Using the magnetoelastic constants for bulk Fe, $\lambda_{001}=20.7\times10^{-6}$ and $\lambda_{111}=-21.2\times10^{-6}$,[20] it can be seen that both energy terms contribute to an uniaxial anisotropy with the [001] direction as the easy axis. Assuming that the stress is the same in the two energy expressions one finds that $E_{001}\gg E_{1\bar{1}0}$. Identifying the first order uniaxial constant K_1 in Eq. (1) with the prefactor in the expression for E_{001}, one obtains $K_1=\frac{3}{2}\lambda_{001}\sigma$. Using the value of K_1 extracted from the magnetization measurement [Fig. 4(a)], λ_{001} (Ref. 20) and the elastic constants[21] for bulk Fe, the strain ε_{001}, in the [001] direction can be calculated. These values give $\varepsilon_{001}\approx 4\%$ to be compared with $\varepsilon_{001}\approx 2\%$ determined from the diffraction experiments. A quantitative comparison between the calculated and the experimental values of the lattice strain is speculative since the magnetoelastic constants λ_{001} and λ_{111}, as well as the elastic constants in a thin film under considerable strain is expected to deviate from the bulk values. Furthermore, Eq. (3) assumes small deviations from cubic symmetry which is not the case in the present samples. However, the magnetoelastic theory qualitatively model a uniaxial behavior of the anisotropy with the easy axis in the [001] direction, as has been found from the magnetization experiments.

C. Transport properties

The main contributions to the magnetotransport properties in multilayers which include a ferromagnetic element arise

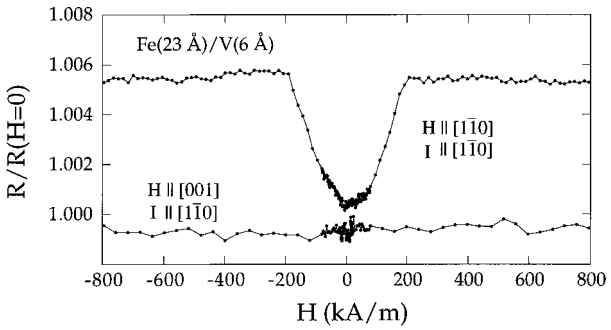

FIG. 5. Reduced electrical resistance $R/R(H=0)$ at 10 K vs applied magnetic field for a Fe (23 Å)/V (6Å) superlattice. The magnetic field is applied in the film plane in the parallel ($H\|[1\bar{1}0]$ and $I\|[1\bar{1}0]$) and in perpendicular ($H\|[001]$ and $I\|[1\bar{1}0]$) orientations.

from the anisotropic magnetoresistance (AMR) (Ref. 22) and in some magnetic multilayers also from the GMR. To quantify the AMR, the spontaneous anisotropic magnetoresistance is defined as

$$(\Delta\rho/\rho)_{\mathrm{AMR}}=(\rho_{\|}-\rho_{\perp})/\rho_0, \tag{4}$$

where $\rho_{\|}$ and $\rho_{\perp}$ are the resistivities when the magnetization direction is parallel or perpendicular to the current I. ρ_0 is the resistivity of the thermally demagnetized state.

In contrast to the AMR effect, the GMR is independent of the in-plane current direction but is, on the other hand, governed by the relative orientation of the magnetization of the ferromagnetic layers in the superlattice. The magnitude of the GMR is usually expressed by the following relation:

$$(\Delta\rho/\rho)_{\mathrm{GMR}}=(\rho_{\uparrow\downarrow}-\rho_{\uparrow\uparrow})/\rho_{\uparrow\uparrow}, \tag{5}$$

where $\rho_{\uparrow\downarrow}$ is the resistivity at antiferromagnetic alignment of the magnetization in the successive ferromagnetic layers and $\rho_{\uparrow\uparrow}$ is the resistivity at saturation (the magnetization in the successive ferromagnetic layers are aligned parallel to the magnetic field). For many multilayered systems $(\Delta\rho/\rho)_{\mathrm{GMR}} \gg (\Delta\rho/\rho)_{\mathrm{AMR}}$.

In Fig. 5 the magnetoresistance at 10 K for the Fe (23 Å)/V (6 Å) superlattice is plotted vs applied field in the parallel ($H\|[1\bar{1}0]$ and $I\|[1\bar{1}0]$) and the perpendicular ($H\|[001]$ and $I\|[1\bar{1}0]$) orientation. In the parallel orientation, the direction of the magnetization is continuously rotated from perpendicular to parallel the current as the field is increased from zero to the saturation field. The increase of the resistance with increasing field in this orientation is a signature of the AMR. When the field is applied in the easy [001] direction, the magnetization is either parallel or antiparallel to the magnetic field. The relative orientation between the current and the magnetization is unchanged during the field cycle and hence the resistivity is constant. A similar influence of the AMR on the total resistance, as illustrated in Fig. 5, was found for all samples with V thicknesses less than 15 Å.

For V thicknesses larger than 15 Å, an influence of the GMR on the magnetoresistive properties is observed. This is illustrated in Fig. 6 where the magnetoresistance is plotted for the Fe (23 Å)/V (21 Å) superlattice in the parallel ($H\|[001]$, $I\|[001]$) [Fig. 6(a)] and in the perpendicular

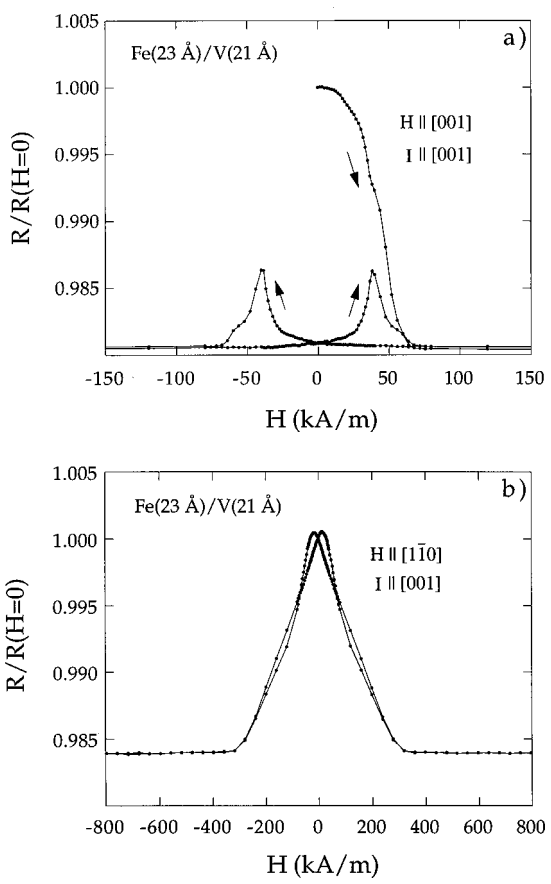

FIG. 6. Reduced electrical resistance, $R/R(H=0)$, at 10 K vs applied magnetic field for a Fe (23 Å)/V (21 Å) superlattice. The magnetic field is applied in the film plane in (a) the parallel ($H\|[001]$ and $I\|[001]$) and in (b) the perpendicular ($H\|[1\bar{1}0]$ and $I\|[001]$) orientation.

($H\|[1\bar{1}0]$, $I\|[001]$) [Fig. 6(b)] orientation. In both orientations the magnetoresistance decreases with increasing field, which is a signature of the GMR effect. No influence of AMR on the magnetoresistance could be observed. As can be seen in Fig. 6(b), the magnitude of the GMR in the perpendicular orientation is approximately 1.6% which is near the value found from the virgin sample measured in the parallel orientation (1.9%). In the parallel orientation the magnitude of the GMR only reaches 0.7%.

The large difference of the GMR effect between the parallel and perpendicular direction in the Fe (23 Å)/V (21 Å) superlattice is due to an interplay between the magnetocrystalline anisotropy, the pinning forces and the exchange coupling that favors an antiparallel alignment of the Fe layers. In the easy direction, the magnetization curve is squarelike with a coercive force of approximately 32 kA/m. The pinning forces have a strong influence on the magnetization loop and the exchange coupling across the V layers has only an influence on the magnetic structure at magnetic field strengths close to the coercive field, where a less complete antiparallel alignment of the moments is achieved. When the magnetic field is reversed after saturation in the hard direction, the magnetic moments will initially, due to the magnetocrystalline anisotropy, undergo a reversible rotation towards the easy directions. During this reversible process the magnetic exchange coupling may be strong enough to impose a nearly

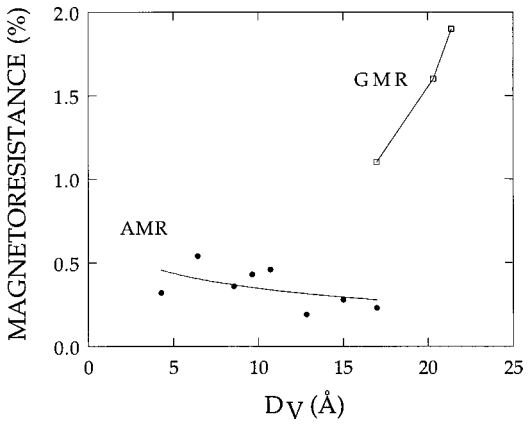

FIG. 7. Magnetoresistance at 10 K vs thickness of the V interlayer D_V for the Fe/V (110) superlattices. The AMR data, defined according to Eq. (4) where $\rho_0 = \rho_\perp$, are extracted from the parallel orientation ($H \| [1\bar{1}0]$ and $I \| [001]$). The GMR data, defined according to Eq. (5), are extracted from thermally demagnetized samples. The lines are guides to the eye.

complete antiparallel structure when the field is reversed to zero. The fact that the GMR in the hard direction is of the same magnitude as found in the virgin sample implies that the successive Fe layers form a nearly complete antiparallel structure at zero magnetic field.

In Fig. 7 the magnitude of the magnetoresistance at 10 K is plotted as a function of the thickness of the V interlayer. The AMR data, defined according to Eq. (4), where $\rho_0 = \rho_\perp$ is the resistivity at zero field, are extracted from measurements with the applied field in the hard direction and parallel to the current ($H \| [1\bar{1}0]$ and $I \| [001]$). The GMR data, defined according to Eq. (5), are extracted from the virgin curve for thermally demagnetised samples. For all V thicknesses less than 16 Å, the anisotropic magnetoresistance governs the magnetoresistive properties. A slight decrease of the AMR with increasing V thickness can be seen. For V thicknesses of approximately 16 Å also the GMR effect is observed in the magnetoresistive data. When further increasing the V thickness, the GMR dominates over the AMR.

DISCUSSION AND SUMMARY

The lattice mismatch between Fe and V causes a tuneable elongation of the in-plane lattice parameter of Fe in Fe/V superlattices. For the Fe/V (110) superlattices the cubic symmetry is broken and a large in-plane uniaxial magnetic anisotropy of magnetoelastic origin develops. In Fe/V (001) superlattices on the other hand, the Fe layers are symmetrically strained and the fourfold crystallographic and magnetocrystalline anisotropy in-plane symmetry retains.[7] In this case the anisotropy energy increases linearly with increasing strain of the Fe layers.

Investigation of the magnetotransport properties on Fe/V (001), with thick Fe,[7] have shown that for V thicknesses up to 20 Å the magnetoresistance is characterized by the AMR. This finding is in contrast to the present result from the Fe/V (110) system in which the GMR effect was found for V thicknesses larger than 15 Å, indicating antiferromagnetic coupling between the Fe layers. The details of this ''orientation dependence'' of the magnetic coupling in Fe/V is, however, unclear. Based on the results from the structural characterization it has been found that the interface roughness is different in the Fe/V (110) and the Fe/V (001) systems, at equal Fe thickness. To determine if the observed ''orientation dependence'' of the magnetic coupling is due to the interface roughness or an intrinsic orientation effect, as suggested in a theoretical model,[5] requires further investigations.

In summary, Fe/V (110) superlattices have been grown on Al_2O_3 (1120) substrates, using Mo and $Mo_{1-x}V_x$ alloy seed layers. The lower limit of the in-plane and out-of-plane crystal coherence is determined to be 300 and 650 Å, respectively, for a 3000 Å thick film. The interface roughness is limited to approximately 2 monolayers. A large in-plane uniaxial anisotropy that dominates the cubic magnetocrystalline anisotropy is observed. The origin of this uniaxial anisotropy is assigned to magnetoelastic effects due to the misfit strain in the superlattice. The magnetotransport measurements show that for V thicknesses less than 15 Å, anisotropic magnetoresistance is present. For larger thicknesses, also giant magnetoresistance effects appear indicating an antiferromagnetically coupled structure. The interplay between the antiferromagnetic coupling, the in-plane uniaxial anisotropy and the hysteresis effects is discussed.

ACKNOWLEDGMENTS

Henk van Greevenbroek is acknowledged for help in evaluating the RHEED patterns and Lynnette D. Madsen for assistance with the XRD measurements. Gabriella Anderson is also acknowledged for assistance in the sample growth. This work has been performed within the Thin Film Consortium and financial support from NUTEK and NFR is gratefully acknowledged.

[1] D. M. Edwards, J. Mathon, R. B. Muniz, and M. S. Phan, Phys. Rev. Lett. **67**, 493 (1991); S. S. P. Parkin, N. More, and K. P. Roche, *ibid.* **64**, 2304 (1990).

[2] B. Dieny, J. Magn. Magn. Mater. **136**, 335 (1994).

[3] K. Baberschke, Appl. Phys. A: Solids Surf. **62**, 417 (1996); F. J. A. Broeder, W. Hoving, and P. J. H. Bloemen, J. Magn. Magn. Mater. **93**, 562 (1991).

[4] G. R. Harp, S. S. P. Parkin, R. F. C. Farrow, R. F. Marks, M. F. Toney, Q. H. Lam, T. A. Rabedeau, and R. J. Savoy, Phys. Rev. B **47**, 8721 (1993); V. S. Speriosu, J. P. Nozieres, B. A. Gurney, B. Dieny, T. C. Huang, and H. Lefakis, *ibid.* **47**, 11 579 (1993); E. Fullerton, D. Kelly, J. Guimpel, I. Schuller, and Y. Bruynseraede, Phys. Rev. Lett. **68**, 859 (1992).

[5] P. Bruno and C. Chappert, Phys. Rev. Lett. **67**, 1602 (1991); **67**, 2592 (1991).

[6] B. D. Hermsmeier, R. F. C. Farrow, C. H. Lee, E. E. Marinero, C. J. Lin, R. F. Marks, and C. J. Chien, J. Appl. Phys. **69**, 5646 (1991).

[7] P. Granberg, P. Nordblad, P. Isberg, B. Hjövarsson, and R. Wäppling, Phys. Rev. B **54**, 1199 (1996).

[8] P. Poulopoulos, P. Isberg, W. Platow, W. Wisny, M. Farle, B. Hjörvarsson, and K. Baberschke, J. Magn. Magn. Mater. **48**, 480 (1997); B. Hjövarsson, J. Dura, P. Isberg, T. Watanabe, T. J. Udovic, G. Andersson, and C. F. Majkratz, Phys. Rev. Lett. **79**, 901 (1997).

[9] J. E. Mattson, E. E. Fullerton, C. H. Sowers, and S. D. Bader, J. Vac. Sci. Technol. A **13**, 276 (1995).

[10] S. Parkin, Phys. Rev. Lett. **67**, 3598 (1991).

[11] P. Grünberg, J. Barnas, F. Saurenbach, J. Fuss, A. Wolf, and M. Vohl, J. Magn. Magn. Mater. **93**, 58 (1991).

[12] Peter Isberg, Ph.D. thesis, Uppsala University, 1997.

[13] P. V. de Weijer and D. K. G. de Boer, Philips J. Res. **47**, 247 (1993).

[14] B. D. Cullity, *Elements of X-Ray Diffraction* (Addison-Wesley, London, 1978), p. 102.

[15] P. Bödeker, A. Abromeit, K. Bröhl, P. Sonntag, N. Metoki, and H. Zabel, Phys. Rev. B **47**, 2353 (1993).

[16] A. Marty, B. Gilles, J. Eymery, A. Chamberod, and J. C. Joud, J. Magn. Magn. Mater. **121**, 57 (1993); H. J. Elmers and U. Gradmann, Appl. Phys. A: Solids Surf. **51**, 255 (1990); B. M. Clemens *et al.*, J. Magn. Magn. Mater. **121**, 37 (1993).

[17] B. Westerstrand, P. Nordblad, and L. Nordborg, Phys. Scr. **11**, 383 (1975).

[18] *American Institute of Physics Handbook* (McGraw-Hill, New York, 1972), pp. 5–208.

[19] S. Chikazumi, *Physics of Magnetism* (Wiley, New York, 1964), p. 183.

[20] E. W. Lee, Rep. Prog. Phys. **18**, 184 (1955).

[21] A. Guy and J. Hren, *Elements of Physical Metallurgy*, 3rd ed. (Addison-Wesley, New York, 1974), p. 52.

[22] I. Campbell and A. Fert, in *Ferromagnetic Materials*, edited by E. P. Wohlfarth (North-Holland, Amsterdam, 1982), Vol. 3.